

This research was originally published in the Journal of Biological Chemistry.

Takeshi Kawai, Yukie Katayama, Linjun Guo, Desheng Liu, Tatsuya Suzuki, Kou Hayakawa, Jae Min Lee, Toshihiro Nagamine, J. Joe Hull, Shogo Matsumoto, Hiromichi Nagasawa, Masaru Tanokura, Koji Nagata. Identification of Functionally Important Residues of the Silkmoth Pheromone Biosynthesis-activating Neuropeptide Receptor, an Insect Ortholog of the Vertebrate Neuromedin U Receptor. *The Journal of Biological Chemistry*. 2014; 289:19150-19163, doi: 10.1074/jbc.M113.488999.

© the American Society for Biochemistry and Molecular Biology.

Identification of Functionally Important Residues of the Silkmoth Pheromone Biosynthesis-Activating Neuropeptide Receptor, an Insect Ortholog of the Vertebrate Neuromedin U Receptor*

Takeshi Kawai (河合岳志)^{‡1}, Yukie Katayama (片山幸江)^{‡1}, Linjun Guo (郭琳珺)[‡], Desheng Liu (刘德生)[‡], Tatsuya Suzuki (鈴木達也)[‡], Kou Hayakawa (早川江)[‡], Jae Min Lee (李載旼)[§], Toshihiro Nagamine (永峰俊弘)[§], J. Joe Hull[¶], Shogo Matsumoto (松本正吾)[§], Hiromichi Nagasawa (長澤寛道)[‡], Masaru Tanokura (田之倉優)^{‡2}, and Koji Nagata (永田宏次)^{‡2}

From the [‡]Department of Applied Biological Chemistry, Graduate School of Agricultural and Life Sciences, The University of Tokyo, 1-1-1 Yayoi, Bunkyo-ku, Tokyo 113-8657, Japan, [§]Molecular Entomology Laboratory, RIKEN Advanced Science Institute, Wako, Saitama 351-0198, Japan, [¶]USDA-ARS Arid Land Agricultural Research Center, Maricopa, AZ, USA

*Running title: *Ligand-Receptor Interactions of PBAN-PBANR and NMU-NMUR*

To whom correspondence should be addressed:

Masaru Tanokura, Department of Applied Biological Chemistry, Graduate School of Agricultural and Life Sciences, The University of Tokyo, 1-1-1 Yayoi, Bunkyo-ku, Tokyo 113-8657, Japan. Tel: +81-3-5841-5165; Fax: +81-3-5841-8023; E-mail: amtanok@mail.ecc.u-tokyo.ac.jp.

Keywords: *Bombyx mori*; class-A GPCR; FXPRXamide motif; ligand-receptor interaction; neuromedin U; peptide hormone; sex pheromone biosynthesis

Background: The moth pheromone biosynthesis-activating neuropeptide (PBAN) and vertebrate neuromedin U (NMU) have a similar biologically essential C-terminal motif (F-X₁-P-R-X₂-NH₂).

Results: Mutation data revealed important residues in the silkmoth PBAN receptor for ligand binding and signaling.

Conclusion: Two glutamate residues conserved in the PBAN/NMU receptor-family of GPCRs are responsible for ligand recognition.

Significance: A novel ligand-receptor interaction is proposed for the PBAN/NMU-family of

neuropeptides and receptors.

SUMMARY

The biosynthesis of sex pheromone components in many lepidopteran insects is regulated by the interaction between pheromone biosynthesis-activating neuropeptide (PBAN) and the PBAN receptor (PBANR), a class-A G-protein-coupled receptor (GPCR). To identify functionally important amino acid residues in the silkmoth PBANR, a series of 27 alanine substitutions were generated using a PBANR chimera C-terminally fused with EGFP. The PBANR

mutants were expressed in Sf9 insect cells and their ability to bind and be activated by a core PBAN fragment (C10PBAN^{R2K}) were monitored. Among the 27 mutants, 23 localized to the cell surface of transfected Sf9 cells, while the other four remained intracellular. Reduced binding relative to wildtype was observed with 17 mutants and decreased Ca²⁺ mobilization responses were observed with 12 mutants. Ala substitution of E95, E120, N124, V195, F276, W280, F283, R287, Y307, T311, and F319 affected both binding and Ca²⁺ mobilization. The most pronounced effects were observed with the E120A mutation. A molecular model of PBANR indicated that the functionally important PBANR residues map to the second, third, sixth and seventh transmembrane helices, implying that the same general region of class-A GPCRs recognizes both peptidic and non-peptidic ligands. Docking simulations suggest similar ligand-receptor recognition interactions for PBAN-PBANR and the orthologous vertebrate pair—neuromedin U (NMU) and NMU receptor (NMUR). The simulations highlight the importance of two glutamate residues, E95 and E120 in silkworm PBANR and E117 and E142 in human NMUR1, in the recognition of the most functionally critical region of the ligands, the C-terminal residue and amide.

The successful propagation of many moth species is dependent on the female's ability to attract conspecific males via species-specific sex pheromones (1,2). These sex pheromone components are predominantly unsaturated,

acyclic, aliphatic C₁₀–C₁₈ compounds containing an oxygenated functional group (e.g. aldehyde, alcohol, or acetate ester). They are synthesized *de novo* in the pheromone gland (specialized tissue located between the eighth and ninth abdominal segments) from acetyl-CoA through fatty acid synthesis with varied desaturation and limited chain-shortening reactions followed by reductive modification of the acyl group (2,3). In the silkworm, *Bombyx mori*, production of the principal sex pheromone component bombykol, (*E,Z*)-10,12-hexadecadien-1-ol, is initiated during photophase starting from the day of adult eclosion (4,5). Like most moth sex pheromones, bombykol is synthesized from acetyl-CoA through palmitate (16:0), but is then stepwise converted to the bioactive compound by Δ11 desaturation, Δ10,12 desaturation, and fatty-acyl reduction to the alcohol (2,6-8).

In most Lepidoptera, pheromone biosynthesis is regulated by a C-terminally amidated 33-amino acid neuropeptide termed pheromone biosynthesis-activating neuropeptide (PBAN)² that originates from the subesophageal ganglion. PBAN was initially isolated in 1989 from the corn earworm *Helicoverpa zea* (9) and *B. mori* (10) and has since been identified in a variety of species (11). Structure-function studies have determined that the minimal sequence necessary for pheromonotropic activity resides in the C-terminal five residues and amide group, F-X-P-R-L-NH₂ (X = S, T, G or V) (12). Several neuropeptides containing the C-terminal F-X-P-R-L-NH₂ motif have been identified from a number of insect orders including Lepidoptera, Diptera and Orthoptera (13). These peptides regulate diverse

biological activities including initiation of *B. mori* embryonic diapause (14), lepidopteran larval melanization (15), ecdysteroidogenesis in the prothoracic gland of *B. mori* (16), hindgut/oviduct contraction in cockroach (17) and locust (18), and acceleration of pupariation in flies (19).

The F-X-P-R-L-NH₂ receptors identified thus far have been characterized as class-A G protein-coupled receptors (GPCRs). The PBAN receptor (PBANR) was first cloned from *H. zea* (20) as an ortholog of the vertebrate neuromedin U receptor (NMUR; 21-24), which recognizes peptides with a C-terminal F-R-P-R-N-NH₂ motif such as neuromedin U (NMU) and neuromedin S (NMS) (25,26). Since then, PBANRs from *B. mori* (27), *Heliothis virescens* (28), *Manduca sexta* (Kim *et al.*, unpublished; GenBank: FJ240221-FJ240224), *Plutella xylostella* (29), *H. armigera* (30), *Spodoptera littoralis* (31), *S. exigua* (32), *Pseudaletia separata* (33), and *Ostrinia nubilalis* (34) have been identified. Functional analyses have shown that PBANR activation triggers an influx of extracellular Ca²⁺ in isolated *B. mori* pheromone glands (35) as well as insect cells transiently expressing PBANR (20,27).

Structure-function studies of PBANRs have revealed a number of intracellular domains and sites crucial for receptor activation and regulation (27,36,37). The roles of the extracellular loops (ECLs) and transmembrane (TM) domains in PBAN binding and signaling, however, have not been as well defined. To begin to elucidate the structural determinants that govern ligand discrimination, Choi and co-workers (38) used a series of domain swaps to implicate ECL3 and the

N-terminus in PBAN-induced activity. Point mutations of a limited number of residues (five in total) implicated S300 and F303 in ECL3 and two potential *N*-glycosylation sites in the N-terminus (38,39). The applicability of those findings to other PBANRs is questionable as a series of truncations that removed the first 27 residues, including the homologous *N*-glycosylation sites, from the *B. mori* PBANR had no effect on cell surface targeting or ligand-induced internalization (37). Molecular modeling and evolutionary trace approaches designed to facilitate identification of the PBAN binding pocket identified a number of potential ligand interaction sites (40,41), many of which map to the ECLs. Those sites, however, have yet to be experimentally verified.

In our current study, we used multiple sequence alignments and PBANR homology modeling to identify 27 amino acid residues in the *B. mori* PBANR sequence as potential ligand interaction sites. To assess their functional roles, the identified residues were Ala-substituted and expressed as PBANR-EGFP fusion proteins in cultured insect cells with their subcellular localization, ligand-binding and ligand-induced mobilization of extracellular Ca²⁺ assessed.

Docking simulations using a homology-based molecular model of PBANR with the solution structure of the minimal active fragment of PBAN (i.e. F-S-P-R-L-NH₂, referred to as C5PBAN) incorporating a type-I β -turn (42-44) were consistent with both mutational data and the degree and nature of sequence conservation across PBANRs and related receptors. Independent docking simulations using human neuromedin U (NMU) with human NMU receptor 1 (NMUR1)

suggested that the ligand-receptor pairs of PBAN-PBANR and NMU-NMUR1 share similar intermolecular interactions. The docking models also suggest that the functionally essential amide and C-terminal residue of both PBAN and NMU interact with two glutamate residues in TM2 and TM3, both of which are highly conserved across the NMUR/PBANR-family of GPCRs.

EXPERIMENTAL PROCEDURES

Homology-based identification of putative ligand interaction sites in PBANR—Homology-based molecular models of the *B. mori* PBANR were constructed using CPHmodels (45), ESyPred3D (46), and Phyre2 (47) with the crystal structures of the human β 2 adrenergic receptor (β 2AR; PDB: 2RH1 (48) and 3D4S (49)) and human A_{2A} adenosine receptor (A_{2A} AR; PDB: 3EML (50)) as templates. The PBANR sequence was then aligned using ClustalW (51) followed by manual adjustments with related GPCRs: *H. zea* PBANR (20), *B. mori* diapause hormone receptor (DHR) (52), *Drosophila melanogaster* pyrokinin-1 and -2 receptors (PK1R (53) and PK2R (54)), and human NMUR-1 and -2 (21-24). The amino acid residues in PBANR that corresponded to the ligand-recognition sites in β 2AR and A_{2A} AR and that were also highly conserved across the PBANR-like GPCRs were mapped onto the homology-based PBANR models. DaliLite (55) was used for sequence alignment based on the crystal structures. Putative ligand interacting residues were identified and targeted for Ala substitution.

Construction of Ala-substituted PBANR-EGFP expression plasmids—The expression plasmid

encoding a chimeric *B. mori* PBANR-EGFP protein was prepared as described (27). Individual Ala substitutions were generated via point mutations using the parental PBANR-EGFP plasmid and the QuikChange (Agilent Technologies, Santa Clara, CA, USA) method. The coding regions of the respective PBANR-EGFP mutants were sequence verified.

Synthesis and purification of PBAN analogs—Reagents for peptide synthesis were purchased from Watanabe Chemical Industries (Hiroshima, Japan). The 10-amino acid peptide S-K-T-R-Y-F-S-P-R-L-NH₂ (termed C10PBAN^{R2K}), which corresponds to the C-terminal 10 amino acids of *B. mori* PBAN, was synthesized on an automated Apex 369 peptide synthesizer (AAPPTec, Louisville, KY, USA) using standard Fmoc solid-phase protocols. To facilitate efficient labeling with Rhodamine Red-X succinimidyl ester (Life Technologies, Carlsbad, CA, USA), an R2K mutation was introduced into the peptide during synthesis. After de-protection and cleavage from the resin, the synthetic C10PBAN^{R2K} peptide was purified by reverse-phase HPLC on a PEGASIL ODS column (10 mm i.d. x 150 mm, Senshu Kagaku, Tokyo, Japan). The peptide was eluted at a flow rate of 4.0 ml/min using a binary solvent system consisting of 0.05% trifluoroacetic acid (TFA) (solvent A) and 90% CH₃CN/0.05% TFA (solvent B). The elution profile began with an isocratic flow of 0% B for 2.5 min, followed by a linear gradient from 0% B to 75% B in 15 min, and ended with a 100% B isocratic flow for 30 min. Tritium-labeled C10PBAN^{R2K} was synthesized by S-[³H]methylation (56) of Cys-C10PBAN^{R2K},

C-S-K-T-R-Y-F-S-P-R-L-NH₂, with [³H]CH₃I (100 mCi/mmol, American Radiolabeled Chemicals, St. Louis, MO, USA). C10PBAN^{R2K} (100 µg, 70 nmol) was dissolved in 1.0 ml of 14% (v/v) DMF, 100 mM NaHCO₃ (pH 8.3) and 5 mM TCEP. Premixed [³H]CH₃I/DMF (4.7 µl and 42 µl) was added to the peptide solution, and incubated at room temperature for 1 h. Then, tritium-labeled C10PBAN^{R2K}, Cys([³H]Me)-C10PBAN^{R2K}, was purified by reverse-phase HPLC.

Confocal scanning laser microscopy—Co-localization of a red fluorescent analog of *B. mori* PBAN, Rhodamine Red-X-labeled C10PBAN^{R2K} (RR-C10PBAN^{R2K}), and the PBANR-EGFP mutants was assessed using a confocal scanning laser microscope. Sf9 insect cells, derived from the fall armyworm *Spodoptera frugiperda* (57,58), were adherently cultured on 35-mm glass bottom dishes (Asahi Glass, Tokyo, Japan) at 28°C for two days with 1000 µl of IPL-41 (Life Technologies) supplemented with 10% FBS (Nichirei Bioscience, Tokyo, Japan). Cells were transfected with 5 µg of each PBANR-EGFP expression plasmid using 10 µl of Cellfectin II (Life Technologies), and incubated at 28°C for 16 h. Transfected cells were washed with 10% FBS/IPL-41 containing 200 µg/ml kanamycin, and incubated at 28°C for 24 h. To examine co-localization of RR-C10PBAN^{R2K} with the PBANR-EGFP mutants, cells were incubated in 500 µl IPL-41 containing 100 nM RR-C10PBAN^{R2K} in the dark at 4°C for 60 min, and then washed three times with PBS and fixed with 4% formaldehyde in PBS. Fluorescence images of PBANR-EGFP and RR-C10PBAN^{R2K} were obtained using a FV-1000D confocal

scanning laser microscope (Olympus, Tokyo, Japan) following excitation at 488 nm (EGFP) and 569 nm (Rhodamine Red). Images obtained correspond to a minimum of 20 individual cells expressing the wildtype and mutant constructs. The fluorescent data were analyzed using Fluoview (Olympus) and statistical analyses performed using a Tukey-Kramer test. These experiments were performed in four replicates such that comparative analyses were performed with data from 80 individual cells.

Ligand binding assay—A radioligand binding assay was performed using the filter plate method (59). Membrane suspensions from Sf9 cells expressing wildtype or a mutant PBANR-EGFP were incubated with different concentrations of Cys([³H]Me)-C10PBAN (100 mCi/mmol) in a buffer containing 500 mM NaCl, 25 mM HEPES-NaOH (pH 7.5) and 1% (w/v) BSA in a total volume of 200 µl for 60 min at room temperature. Unbound radioligand was removed by rapid filtration through a GF/F filter (GE Healthcare, Pollards Wood, UK) presoaked in 0.3% (v/v) polyethyleneimine, and the filter was rinsed twice with 1 ml of ice-cold buffer. Each filter was placed in a scintillation vial and 5 ml of scintillation cocktail added. The filter-bound radioactivity was measured using the liquid scintillation counter (LSC-6100, Aloka, Tokyo, Japan). Nonspecific binding was determined in parallel reaction in the presence of 200 µM unlabeled Cys(Me)-C10PBAN. Equilibrium dissociation constants (K_d) for Cys([³H]Me)-C10PBAN were calculated by non-linear curve fitting to the saturation curves using IGOR Pro (WaveMetrics, Lake Oswego, OR,

USA).

Confocal scanning laser microscopy-based Ca^{2+} imaging assay—Sf9 cells were harvested and incubated in a 24-well glass bottom plate (Asahi Glass) at 28°C for two days in 500 μ l of IPL-41 medium supplemented with 10% FBS. Cells were transfected overnight with 1 μ g plasmid DNA in 250 μ l IPL-41 and 2.5 μ l of Cellfectin II (Life Technologies). On the day of the experiment, cells were washed three times with 500 μ l IPL-41 and then incubated in the dark at 28°C for 30 min with 250 μ l IPL-41 supplemented with 0.75 μ l each of Pluronic F-127 (Life Technologies) and Fura Red AM (1 mM stock; Life Technologies). After incubation, the cells were washed three times with 500 μ l IPL-41, and then maintained in the dark at 28°C for 20 min with 300 μ l IPL-41 to allow hydrolysis of the Fura Red AM ester bond. The fluorescence intensities of EGFP and Fura Red were measured using a FV-1000D confocal laser microscope following excitation at 488 nm and 548 nm, respectively. To measure the Ca^{2+} mobilization responses of PBANR-EGFP and the Ala-substitution mutants, fluorescence at 509 nm and 610 nm was monitored over 40 scans (1.08 sec/scan) following addition of 100 μ l C10PBAN^{R2K} to each well after 10 scans. Fura Red fluorescence was analyzed using Fluoview software. The data obtained from five replicates were statistically analyzed using a Tukey-Kramer test.

Molecular modeling and docking simulation of PBAN-PBANR and

NMU-NMUR—Homology-based molecular models of PBANR were constructed using the Molecular Operating Environment (MOE)

software suite (Chemical Computing Group, Montreal, Canada) with the crystal structures of agonist-bound turkey β 1 adrenergic receptor (β 1AR; PDB: 2Y03 (60)) and human A_{2A} adenosine receptor (A_{2A} AR; PDB: 3QAK (61)), used as templates. Docking simulations of PBAN with PBANR were performed using AutoDock Vina (62) with PBANR conformations in which the N- and C-terminal ends of TM1–5 and TM6–7, respectively, were opened and separated by 0, 1, 2, 3, 4, and 5 Å. In the docking simulation, a subset of the functionally important PBANR residues were defined as flexible residues: E95, E120, N124, S207, F211, F212, F276, W280, F283, H284, and R287. The PBAN molecular model was restricted to the minimal C-terminal active core (F-S-P-R-L-NH₂, C5PBAN) and was derived from the NMR solution structure of C10PBAN dissolved in 30% (v/v) TFE-*d*₃ in 50 mM sodium phosphate buffer (pH 6.0) and 0.02% (w/v) sodium azide. Under these conditions, the C-terminal four residues form a type-I β -turn whereas the N-terminal five residues are highly disordered (44). These latter residues are not essential for PBAN activity and were not used in the docking simulation. An acetyl group was added to the N-terminus of C5PBAN *in silico* to avoid unfavorable interactions by the N-terminal α -amino group that does not exist in the full-length PBAN.

Homology-based molecular models of human NMUR1 were constructed based on the crystal structures of agonist-bound turkey β 1AR and A_{2A} AR as described above. The molecular model of the C-terminal active core of NMU, F-R-P-R-N-NH₂, termed C5NMU, was

constructed based on the C5PBAN molecular model. The docking simulation of C5NMU to NMUR1 was performed with AutoDock Vina as described. Intermolecular interactions in the docking models were analyzed with PISA (63) and visualized with PyMOL (64).

RESULTS

Prediction of PBANR ligand recognition sites—Knowledge of GPCR three-dimensional structures can provide mechanistic insights into ligand binding and aid in the determination of ligand interaction sites. To facilitate identification of these sites in PBANR, we aligned the *B. mori* PBANR sequence with related GPCRs (*H. zea* PBANR, *B. mori* DHR, *D. melanogaster* PK1R and PK2R, and human NMUR-1 and -2) and two class-A GPCRs, human β 2AR and human A_{2A}AR, whose ligand recognition residues have been identified. The potential three-dimensional spatial coordinates of the conserved residues were then approximated using a homology-based molecular model of *B. mori* PBANR generated from the human β 2AR (PDB: 2RH1 and 3D4S) and human A_{2A}AR (PDB: 3EML) crystal structures. These sites were then compared with known ligand recognition sites in the two human receptors to identify 27 amino acids residues that potentially comprise the *B. mori* PBANR ligand-binding pocket (Fig. 1). These amino acids are predicted to reside in: TM2 (E95); ECL1 (W100, Y105 and I113); TM3 (S119, E120 and N124); ECL2 (V195, K196, V200, and H201); TM5 (S207, F209, F211, and F212); TM6 (F276, W280, F283, H284 and R287); ECL3 (F303); and TM7 (Y307, T311, F312, G315, Y318 and F319). The functional

importance of these amino acids was evaluated using a PBANR-EGFP chimera in which the 27 candidate residues were systematically replaced with the small hydrophobic amino acid, Ala. The effects of the individual substitutions on cell surface localization, binding of a fluorescent PBAN analog (RR-C10PBAN^{R2K}), and mobilization of extracellular Ca²⁺ in response to C10PBAN^{R2K} were examined in cultured insect Sf9 cells transiently expressing the respective mutants.

Cell surface localization—Most of the mutants localized to the plasma membrane as evidenced by a ring of EGFP-associated fluorescence at the cell surface. In contrast, the fluorescence profile of the S207A, F211A, F212A and H284A mutants was largely intracellular (Fig. 2). S207, F211, and F212 are predicted to reside within TM5 while the fourth residue, H284A, is predicted to be part of TM6. The impaired localization observed with Ala substitution of these residues suggests that their side chains may play a role in stabilizing the PBANR conformation for transport to the plasma membrane.

Binding of a red fluorescent PBAN analog—To examine the ligand-binding ability of each Ala-substituted PBANR-EGFP, Sf9 cells transiently expressing the individual mutants were incubated with RR-C10PBAN^{R2K}, a red fluorescent PBAN analog. A total of 80 cells for each construct (wildtype or the individual mutant PBANR-EGFP) were observed using a confocal scanning laser microscope using excitation wavelengths at 488 nm and 560 nm for EGFP and Rhodamine Red, respectively. Co-localization of the green and red fluorescence signals was

considered an indication of ligand binding (Fig. 2). Variations in receptor expression can affect the degree of ligand binding such that low receptor expression would result in fewer sites for ligand interaction and thus yield a phenotype indistinguishable from loss of a ligand-receptor binding site. To address this issue, we used total cellular EGFP fluorescence as a means of quantifying PBANR expression (Fig. 3A). Based on this metric, we found that expression of the mutants, irrespective of their subcellular localization, was largely comparable to that of wildtype PBANR-EGFP with deviations that did not exceed more than two-fold. We next assessed the affinity of each mutant for the RR-C10PBAN^{R2K} ligand by determining the fluorescence ratio of Rhodamine Red to EGFP at the edge of the cell (Fig. 3B). To insure sufficient fluorescence intensity, a high RR-C10PBAN^{R2K} concentration (100 nM) was used. As expected, the four mutants (S207A, F211A, F212A, and H284A) with impaired cell surface localization had minimal RR-C10PBAN^{R2K} binding. Markedly diminished (statistical significance at $P < 0.01$) RR-C10PBAN^{R2K} binding was observed for 14 mutants (E95A in TM2; E120A and N124A in TM3; V195A in ECL2; F209 in TM5; F276A, W280A, F283A, and R287A in TM6; F303A and Y307A in ECL3; T311A, G315A, and F319A in TM7). This dramatic reduction in binding suggests that these residues may be critical for ligand recognition. An approximate 50% reduction in ligand binding was observed for Y105A (ECL1), K196A (ECL2), and F312A (TM7), suggesting that they may help coordinate ligand recognition. The W100A, I113A, S119A, V200A, H201A, and

Y318A mutations had negligible effects on ligand binding. Furthermore, the poor RR-C10PBAN^{R2K} binding was not correlated with PBANR-EGFP expression (see F209A in Fig. 3A, B), indicating that the impaired binding was specific to the nature of the Ala substitution and not to the degree of expression.

Binding of a radiolabeled PBAN analog—To validate the fluorescence-based binding data, quantitative ligand-binding analyses using tritium-labeled C10PBAN^{R2K} were performed with wildtype PBANR-EGFP and three mutants (E95A, I113A and E120A). The criteria for selecting the mutants used in the assay were based on their observed binding effects and spatial distribution. The TM residing E95A and E120A mutations both had significant effects on ligand binding (Fig. 3B), whereas the I113A mutation, which is predicted to comprise a portion of ECL1, had no effect. The binding isotherms (Fig. 3C) for both wildtype PBANR-EGFP and the I113A mutation were saturating with comparable B_{\max} values (wildtype – 1.4 nM; I113A – 1.2 nM) and K_d values (wildtype – 240 nM; I113A – 110 nM), indicating that the cell surface expression levels of the receptors and affinities for the radiolabeled ligand were similar. In contrast, we were unable to generate binding isotherms for the E95A and E120A mutants (Fig. 3C) despite receptor expression levels comparable to that of wildtype, indicating that the E95A and E120A mutations effectively inhibited specific binding of the radiolabeled ligand. These findings are consistent with the fluorescence-based binding data shown in Fig. 3B.

Ligand-induced Ca^{2+} mobilization—We next

sought to examine the effects of the Ala substitutions on PBANR activation. Previous reports have demonstrated that PBAN-induced activation of heterologously expressed PBANR triggers an influx of extracellular Ca^{2+} (20,27). We consequently used intracellular Ca^{2+} imaging to assess the effects of the Ala substitutions in response to varying concentrations (1, 10 and 100 nM) of C10PBAN^{R2K} (Fig. 4). A comparison of the wildtype PBANR-EGFP K_d (240 nM, Fig. 3C) and EC_{50} (< 0.1 nM, Fig. 4B) indicates that the receptor was sufficiently overexpressed such that only a small fraction of cell surface receptor was required for maximal signaling. The comparable expression levels with wildtype PBANR-EGFP (Fig. 3A) suggests similar conclusions could be drawn for the mutants. This explains why the cells expressing the F212A mutant, which exhibited impaired cell surface localization (Fig. 2), had a moderate Ca^{2+} response (Fig. 4C); some portion of the receptor translocated to the cell surface but was below our threshold of detection (i.e. fluorescent visualization). Consistent with our previous findings, the fluorescence changes associated with Ca^{2+} mobilization (Fig. 4A) in cells expressing the E120A, S207A, and F211A mutations were essentially undetectable at all three ligand concentrations tested. The reduced Ca^{2+} mobilization profiles of cells expressing the E95A, E120A, N124A, F276A, W280A, F283A, R287A, Y307A, and F319A mutants (Fig. 4C), suggests a critical role for these residues in PBANR activation. In contrast, Ca^{2+} mobilization in cells expressing the V195A, T311A, and Y318A mutants was only moderately reduced compared to control cells (Fig. 4C), suggesting a secondary role

for these residues in transmitting the PBAN signal. The intracellular fluorescence of cells expressing the remaining eleven mutants (i.e. W100A, Y105A, I113A, S119A, K196A, V200A, H201A, F209A, F303A, F312A, and G315A) was indistinguishable from control cells, indicating that these residues likely do not contribute to receptor activation.

Homology-based molecular modeling of PBANR and location of functionally important residues—To examine the intramolecular location of the functionally important residues in PBANR in relation to a bound ligand, a second set of homology-based models were constructed using the crystal structures of thermostabilized turkey β 1AR with bound isoprenaline (PDB: 2Y03) and human $\text{A}_{2\text{A}}$ AR with bound UK-432097 (PDB: 3QAK). The resulting models (Data S1) diverged significantly with an RMSD of 3.2 Å for C^α atoms and ligand-docking simulations (see below) were only successful with the $\text{A}_{2\text{A}}$ AR-derived model. Consequently, we used the $\text{A}_{2\text{A}}$ AR-derived model to map the functionally important PBANR residues (Fig. 5). The four residues essential for the efficient localization of PBANR to the plasma membrane (i.e. S207, F211, F212, and H284) clustered within a spatially limited region of TM5 and TM6 (Fig. 5A). Similarly, the residues critical for ligand binding and signaling clustered together with the putative ligand-binding pocket in the three-dimensional model (Fig. 5B, C). Intriguingly, most of the PBANR residues critical for C10PBAN^{R2K} binding and signal transduction share the same general spatial coordinates as the ligand-binding residues in $\text{A}_{2\text{A}}$ AR, β 2AR, β 1AR, and D3 dopamine receptor (D3DR) (65). The ligand-binding residues of neurotensin receptor-1

(NTSR1) (66), however, only partially overlap with PBANR and the above-mentioned class-A GPCRs (Figs. 5D and S1).

Docking simulation of PBAN with PBANR—Finally, to gain insights into PBAN binding itself, we used AutoDock Vina to simulate binding of C5PBAN (F29-S30-P31-R32-L33-NH₂), the smallest active fragment of PBAN (12), with the PBANR homology models generated from the UK-432097 bound A_{2A}AR structure. We were in particular interested in the molecular interactions between C5PBAN and the residues we determined experimentally to be critical for binding and activation. Simulations were performed using C5PBAN with a type-I β turn as NMR studies of PBAN have suggested that the C-terminal active site of PBAN adopts a β -turn (42-44). The ligand-binding pocket of the PBANR molecular models, however, was too small to fully accommodate C5PBAN with the type-I β -turn conformation. We consequently artificially widened the pocket by splitting the N- and C-terminal parts of PBANR (i.e. TM1–5 and TM6–7, respectively) and expanded the gap by 1, 2, 3, 4, or 5 Å. This split GPCR method was selected based on a report demonstrating that the N- and C-terminal regions of β 2AR corresponding to TM1–5 and TM6–7, respectively, form a functional β 2AR when co-expressed (67). The following criteria were used to evaluate reasonable docking models: 1) the ligand-receptor interaction is favorable in terms of binding energy, 2) the bound ligand is accommodated in the ligand-binding pocket of the receptor, 3) the bound ligand interacts with the functionally important residues of the receptor, and 4) the N-terminus of

the ligand extends beyond the entrance of the ligand-binding pocket. With a receptor separation of ≤ 2 Å, no docking model met the above criteria. An appropriate docking model with an affinity of -10.1 kcal/mol was obtained using a 3-Å separated conformation derived from the A_{2A}AR template. This docking model (Data S2) was chosen as the most appropriate because it met all the above criteria with a minimal receptor separation. In the docking model, a number of contact points were observed between C5PBAN and PBANR (Fig. 6A, C and Data S3): F29 – 6 contact points in TMs 6 and 7; S30 – 5 contact points in TMs 6 and 7; P31 – 7 contact points in TMs 5, 6, and 7; R32 – 8 contact points in TMs 3, 5, 6, and 7; L33 – 5 contact points in TMs 2, 3, 6, and 7; and the terminal NH₂ – 3 contact points in TMs 2 and 7. Intriguingly, while no interactions were observed between C5PBAN and the extracellular loops (ECLs), all four residues important for the normal transport of PBANR (i.e. S207, F211, F212, and H284) to the plasma membrane were predicted to interact with C5PBAN, suggesting that these residues may also be crucial for ligand recognition.

Docking simulation of NMU to NMUR—To validate the PBAN-PBANR docking model, we performed a similar simulation using human NMU and human NMUR1, the vertebrate ortholog pair of PBAN and PBAN. NMU has been implicated in the regulation of smooth-muscle contraction, blood pressure and local blood flow, ion transport in the gut, stress responses, cancer, gastric acid secretion, pronociception, and feeding behavior (68). Human NMU is a 25 amino acid peptide with a PBAN-like C-terminal motif,

F21-R22-P23-R24-N25-NH₂ (portions of the sequence identical between PBAN and NMU are underlined), that is highly conserved across a number of vertebrate species and is critical for biological activity (68). Human NMU binds to two receptor types, NMUR1 and NMUR2. For the docking simulation, we modeled the C-terminal five residues and amide of NMU (C5NMU) with a type-I β -turn similar to C5PBAN, and generated homology models of NMUR1 using the same structural templates (PDB: 2Y03 and 3QAK; Data S4) as those used to construct the PBANR models. The same criteria for evaluating reasonable docking models were used. An appropriate docking model with an affinity of -10.7 kcal/mol was obtained using a 2-Å separated NMUR1 model derived from the A_{2A}AR template. This docking model (Data S5) was chosen as the most appropriate because it met all the above criteria with a minimal receptor separation. Inspection of the predicted C5NMU-NMUR1 contact residues revealed significant conservation with those predicted for C5PBAN and PBANR (Fig. 6B, C and Data S6): F21 – 4 contact residues in TMs 6 and 7; R22 – 6 contact residues in TMs 5, 6, and 7; P23 – 8 contact residues in TMs 5, 6, and 7; R24 – 8 contact residues in TMs 3, 5, 6, and 7; N25 – 8 contact residues in TMs 2, 3, 5, 6, and 7; and the terminal NH₂ – 4 contact residues in TMs 2, 6, and 7. Similar to C5PBAN and PBANR, no interactions were seen between C5NMU and the ECLs of NMUR1. The observed conservation in the number, location, and physicochemical properties of the predicted interactions comprising the putative PBANR and NMUR1 binding pockets supports the validity of these docking models.

Comparison of class-A GPCR agonist-recognition residues—To obtain a clearer picture of the ligand binding pocket across multiple class-A GPCRs, the three-dimensional conformations of the ligand bound PBANR (Fig. 7A) and NMUR1 (Fig. 7B) homology models were compared with agonist-bound crystal structures (Fig. 7C-E) of β 1AR (agonist: isoprenaline; PDB: 2Y03), A_{2A}AR (agonist: UK-432097; PDB: 3QAK) and the neurotensin receptor 1 (NTSR1; agonist: neurotensin 8–13; PDB: 4GRV). The difference in sizes of the bound ligands in β 1AR and A_{2A}AR suggests a structural reason why A_{2A}AR proved to be the more suitable template for generating the PBANR and NMUR1 models (Fig. 7A-D). In the NTSR1 structure (Fig. 7E), the C-terminal, biologically active fragment of the peptide hormone neurotensin (R-R-P-Y-I-L-OH, termed C6NTS) is bound. Unlike the molecular models of C5PBAN and C5NMU, this peptide agonist does not form a β -turn but rather adopts an extended conformation with its C-terminus oriented towards the receptor core. The bound C6NTS, however, does not penetrate as deeply into the receptor as the bound ligands in the β 1AR and A_{2A}AR crystal structures or the PBANR and NMUR docking models. Intriguingly, the locations of the agonist-recognition sites are well conserved across PBANR, NMUR, A_{2A}AR, and β 1AR (Fig. 7A-D), but less so for NTSR1 (Fig. 7E). The physicochemical properties of the side chains that comprise the agonist-recognition sites though are exceedingly varied across the GPCRs with only F276 and W280 (PBANR numbering) conserved. This diversity of ligand-recognition residues in terms of location within the receptor helical

bundle and side chain functionalities likely reflects the diverse array of ligands recognized by class-A GPCRs.

DISCUSSION

Neuropeptides mediate numerous biological events in both vertebrates and invertebrates. Intriguingly, despite millions of years of evolutionary divergence, subsets of neuropeptides from these two diverse groups are characterized by similar biologically relevant motifs. One such assemblage of peptides includes the NMU/NMS and the Insecta F-X-P-R-L-NH₂ peptides (i.e. PBAN, DH, melanization and reddish coloration hormone and pyrokinin), both of which share a C-terminal F-X₁-P-R-X₂-NH₂ motif as the active core (68-70). Based on these sequence similarities, and those between certain mammalian receptors and putative GPCRs in the *Drosophila* genome, Hewes and Taghert (71) postulated that peptide ligands with a C-terminal P-R-X-NH₂ motif co-evolved with their respective receptors. They suggested that PBAN-like peptides could interact with receptors exhibiting sequence similarity to mammalian NMURs. Park and co-workers (72) extended this hypothesis and demonstrated that *H. zea* PBAN activated a *Drosophila* GPCR with high similarity to NMUR. Reciprocal experiments measuring the *in vivo* effects of NMU in *H. zea* revealed that the mammalian peptide stimulated pheromone production (20). The fact that NMU can activate PBANR suggests that the PBANR and NMUR binding pockets are similar.

An initial effort to model the structural features of the *H. zea* PBANR on the bovine rhodopsin crystal structure identified 20 residues that

potentially comprise the inner side of the binding pocket (40). Experimental verification of those sites, many of which map to the extracellular domains, has yet to be demonstrated. Furthermore, the utility of using the rhodopsin structure as a starting point for GPCR homology building can be problematic (73-75). Mutational studies designed to identify specific ligand interacting residues in the PBANR pocket have likewise yielded mixed results. Domain swaps of the *H. zea* PBANR ECLs suggested roles for ECL3 and the N-terminus in ligand binding (38). Site-directed mutagenesis of five residues (two in the N-terminus, three in ECL3) within these regions implicated potential N-terminal *N*-glycosylation sites and ECL3 residues S300 and F303 (38,39). The impaired PBAN-induced Ca²⁺ response in those mutational studies though could have resulted from reduced representation at the cell surface due to compromised trafficking, altered stability of the binding pocket, and/or impaired signaling as well as reduced ligand binding. Moreover, incremental truncations of the *B. mori* PBANR N-terminus, which removed homologous *N*-glycosylation sites, had no effect on cell surface localization or PBAN-induced receptor internalization, a regulatory process dependent on functional PBANR signaling (37).

To begin to address some of these discrepancies, we sought to combine molecular modeling techniques with mutational analyses to generate a more robust characterization of the PBANR binding pocket. We mapped the conserved residues from multiple PBANRs and PBANR-like receptors onto homology-based models of the *B. mori* sequence that were built using spatial

coordinates derived from the crystal structures of two GPCRs. This approach facilitated the identification of 27 residues that potentially comprise the putative PBAN ligand-binding pocket. The number and location of the residues identified by our mapping approach differ substantially from those previously predicted to comprise the putative PBAN binding pocket. Only 3 of the 20 potential identified in the rhodopsin-based model of the *H. zea* PBANR (40), were also identified in our study. In contrast, all of the residues identified based on evolutionary trace analysis of PBANR-related sequences (41) are represented in our prediction. The predictive power of that analysis, however, was limited to 11 potential PBANR interacting sites.

The role the 27 residues have on cell surface trafficking of PBANR, ligand binding, and PBAN-induced Ca^{2+} mobilization was assessed via sequential Ala substitutions. Four point mutants (S207A, F211A, F212A, and H284A) impeded PBANR trafficking to the plasma membrane (Fig. 2). Based on our homology model, these four residues, which are located in TM5 (S207A, F211A, and F212A) and TM6 (H284A), are predicted to contribute to a number of inter-helix interactions (Fig. 5A): S207 with R287 (TM6); F211 with three residues in TM3 (N124, V127, and L128) and two residues in TM4 (F166, and T170); F212 with one residue in TM3 (V127) and four residues in TM6 (F276, W280, A281, and H284); and H284 with three residues in TM5 (S208, F212, and V213). These interactions strongly suggest that these side chains are important for stabilizing the PBANR conformation and imply that the observed defect in plasma

membrane trafficking was attributable to impaired PBANR folding. Indeed, the fluorescence profile of the four mutants was strikingly reminiscent of that seen with endoplasmic reticulum localization (76). Docking simulations suggested that these four residues might also be involved in ligand recognition as C5PBAN contacted all four in the docking model. Consistent with this model, the corresponding residues in $\text{A}_{2\text{A}}\text{AR}$, $\beta 1\text{AR}$, and $\beta 2\text{AR}$ are also involved in ligand recognition (Fig. 5D).

Significantly reduced ligand binding and Ca^{2+} mobilization were seen with 11 point mutants, (E95A, E120A, N124A, V195A, F276A, W280A, F283A, R287A, Y307A, T311A, and F319A). In contrast, three mutants (F209A, F303A, and G315A) exhibited defects in lowered binding while a single mutant (Y318A) was defective only in the Ca^{2+} response (Figs. 3 and 4). Surprisingly, despite exhibiting reduced binding, the Ca^{2+} response profile of cells expressing the F209A, F303A, and G315A mutants was comparable to wildtype cells, suggesting that a sufficient amount of ligand had bound to trigger a Ca^{2+} response. The Y318A mutant is the only mutant with normal ligand binding but impaired signaling abilities, indicating that this tyrosine side chain may be important for the putative conformational change induced in response to PBAN binding. F212, F276, W280, F283, and F319 are highly conserved in class-A GPCRs (Fig. 5D), and are involved in formation of the receptor active conformation (77). This likely accounts for the conservation observed in our initial alignments and suggests that they may not necessarily be directly involved in ligand binding. The effects of the mutations could be

allosteric rather than impairing ligand recognition. N124 and F212, which are located deep within the core of the receptor, may likewise have allosteric roles that contribute indirectly to ligand binding.

Our decision to model the backbone conformation of C5PBAN/C5NMU as a type-I β -turn was based on NMR structural analyses of PBAN (43,44) and a pheromonotropic eight-residue cyclic peptide containing a highly similar sequence to C5PBAN (underlined), cyclo(-N-T-S-F-T-P-R-L-) (42,44). The docking simulations of C5PBAN-PBANR and C5NMU-NMUR1 highlighted the functional relevance of this conformation in both PBAN and NMU binding. Although artificial widening by 2–3 Å was required (Fig. 6), the C-terminal active core of both peptides was largely accommodated by the ligand-binding pocket of the respective receptors. In contrast, the full-length peptide hormones (33 amino acids in PBAN and 25 amino acids in NMU) would be sterically hindered from entering the size-limited ligand-binding pockets. As a consequence, the N-terminal flanking regions of C5PBAN and C5NMU, which are not biologically necessary, are proposed to interact with the respective receptor ECLs to strengthen ligand affinity. These varying contact points could potentially function as a selectivity filter for differentiating between ligands with similar active core sequences (e.g. PBAN and DH). In support of this, two residues located in the ECLs, V195 (ECL2) and F303 (ECL3) appear to be important for C10PBAN^{R2K} binding (Figs. 3 and 5*B, D*), but are not C5PBAN interacting sites in the docking model (Fig. 6*A, C*). Five neuropeptides with the C-terminal F-X-P-R-L-NH₂ motif have been

identified in *B. mori* (78), two of which, PBAN and DH, regulate different biological activities and bind two different but homologous receptors, PBANR and DHR. When the functionally important residues of PBANR and the corresponding residues of DHR are compared, all the residues are identical except for V195/Q (ECL2), F303/P (ECL3), and F319/Y (TM7) (Fig. 5*D*), which supports the hypothesis that the ECLs of PBANR, DHR, and related GPCRs function as a ligand selection filter (this study and 38).

The most biologically essential region of the F-X-P-R-L-NH₂ ligand comprises the C-terminal Leu and the associated amide (70). In the docking models of C5PBAN-PBANR and C5NMU-NMUR, this region interacts with conserved residues in PBANR and NMUR1 located in TM2 (E95/E117), TM3 (E120/E142), TM6 (F283/F313) and TM7 (Y318/F345 and F319/Y346) (Fig. 6). The two glutamate residues in TM2 (E95/E117) and TM3 (E120/E142), appear to be critically important for ligand binding in PBANR and are completely conserved in the PBANR/NMUR family of class-A GPCRs. Interestingly, these two glutamate residues, which are characteristic of PBANR/NMUR-related GPCRs, are not as highly conserved across other class-A GPCRs (Figs. 5*D* and S1).

The positions of the putative ligand-binding residues in PBANR are highly conserved with the ligand-binding residues in non-peptidic class-A GPCRs (A_{2A}AR, β 1AR, β 2AR, and dopamine D3 receptor), but not with those of NTSR1, a class-A peptide ligand GPCR (Figs. 5*D*, 7, and S1). Thus, class-A GPCRs can recognize various ligands, both peptidic and non-peptidic, in distinctive

manners using varied residues at different positions.

In summary, the results obtained in this study indicate that the ligand-binding pocket of PBANR/NMUR and related GPCRs recognizes the β -turn conformation of their peptidic ligands and that this pocket, similar to non-peptidic ligand class-A GPCRs, is buried relatively deep within the receptor helical bundle. The specific ligand-binding residues, however, are not conserved, which could account for the multitude of ligands recognized by class-A GPCRs. In

addition, two glutamate residues in PBANR and NMUR1, E95/E117 (TM2) and E120/E142 (TM3), were shown to be critically important for ligand binding and signal transduction, and are proposed to be involved in the recognition of the C-terminal amide and the C-terminal residue of both PBAN and NMU. Our results and simulation data have significantly broadened our understanding of the molecular interactions underlying peptidic ligand interactions with class-A GPCRs, in particular those between PBAN-PBANR and NMU-NMUR.

REFERENCES

1. Roelofs, W. L., and Bjostad, L. B. (1984) Biosynthesis of lepidopteran pheromones. *Bioorg. Chem.* **12**, 279–298
2. Roelofs, W. L., and Rooney, A. P. (2003) Molecular genetics and evolution of pheromone biosynthesis in Lepidoptera. *Proc. Natl. Acad. Sci. U. S. A.* **100**, 9179–9184
3. Tillman, J. A., Seybold, S. J., Jurenka, R. A., and Blomquist, G. J. (1999) Insect pheromones—an overview of biosynthesis and endocrine regulation. *Insect Biochem. Mol. Biol.* **29**, 481–514
4. Ando, T., Hase, R., Funayoshi, A., Arima, R., and Uchiyama, M. (1988) Sex pheromone biosynthesis from ^{14}C -hexadecanoic acid in the silkworm moth. *Agric. Biol. Chem.* **52**, 141–147
5. Fónagy, A., Yokoyama, N., and Matsumoto, S. (2001) Physiological status and change of cytoplasmic lipid droplets in the pheromone-producing cells of the silkworm, *Bombyx mori* (Lepidoptera, Bombycidae). *Arthropod Struct. Dev.* **30**, 113–123
6. Ando, T., Hase, R., Arima, R., and Uchiyama, M. (1988) Biosynthetic pathway of bombykol, the sex pheromone of the female silkworm moth. *Agric. Biol. Chem.* **52**, 473–478
7. Moto, K., Yoshiga, T., Yamamoto, M., Takahashi, S., Okano, K., Ando, T., Nakata, T., and Matsumoto, S. (2003) Pheromone gland-specific fatty-acyl reductase of the silkworm, *Bombyx mori*. *Proc. Natl. Acad. Sci. U. S. A.* **100**, 9156–9161
8. Moto, K., Suzuki, M. G., Hull, J. J., Kurata, R., Takahashi, S., Yamamoto, M., Okano, K., Imai, K., Ando, T., and Matsumoto, S. (2004) Involvement of a bifunctional fatty-acyl desaturase in the biosynthesis of the silkworm, *Bombyx mori*, sex pheromone. *Proc. Natl. Acad. Sci. U. S. A.* **101**, 8631–8636
9. Raina, A., Jaffe, K., Kempe, T. G., Keim, P., Blacher, R. W., Fales, H. M., Riley, C. T., Klun, J. A.,

- Ridgway, R. L., and Hayes, D. K. (1989) Identification of a neuropeptide hormone that regulates sex pheromone production in female moths. *Science* **244**, 796–798
10. Kitamura, A., Nagasawa, H., Kataoka, H., Inoue, T., Ando, T., and Suzuki, A. (1989) Amino acid sequence of pheromone-biosynthesis-activating neuropeptide (PBAN) of the silkworm, *Bombyx mori*. *Biochem. Biophys. Res. Commun.* **163**, 520–526
 11. Rafaeli, A. (2009) Pheromone biosynthesis activating neuropeptide (PBAN): regulatory role and mode of action. *Gen. Comp. Endocrinol.* **162**, 69–78
 12. Kuniyoshi, H., Nagasawa, H., Ando, T., Suzuki, A., Nachman R. J., and Holman, G. M. (1992) Cross-activity between pheromone biosynthesis activating neuropeptide (PBAN) and myotropic pyrokinin insect peptides. *Biosci. Biotechnol. Biochem.* **56**, 167–168
 13. Predel, R., and Wegener, C. (2006) Biology of the CAPA peptides in insects. *Cell. Mol. Life Sci.* **63**, 2477–2490
 14. Imai, K., Konno, T., Nakazawa, T., Komiya, T., Isobe, M., Koga, K., Goto, T., Yaginuma, T., Sakakibara, K., Hasegawa, K., and Yamashita, O. (1991) Isolation and structure of diapause hormone of the silkworm, *Bombyx mori*. *Proc. Japan Acad.* **67B**, 98–101
 15. Matsumoto, S., Kitamura, A., Nagasawa, H., Kataoka, H., Orikasa, C., Mitsui, T., and Suzuki, A. (1990) Functional diversity of a neurohormone produced by the suboesophageal ganglion: molecular identity of melanization and reddish colouration hormone and pheromone biosynthesis activating neuropeptide. *J. Insect Physiol.* **53**, 752–759
 16. Watanabe, K., Hull, J. J., Niimi, T., Imai, K., Matsumoto, S., Yaginuma, T., and Kataoka, H. (2007) FXPRL-amide peptides induce ecdysteroidogenesis through a G-protein coupled receptor expressed in the prothoracic gland of *Bombyx mori*. *Mol. Cell Endocrinol.* **273**, 51–58
 17. Nachman, R. J., Holman, G. M., and Cook, B. J. (1986) Active fragments and analogs of the insect neuropeptide leucopyrokinin: structure-function studies. *Biochem. Biophys. Res. Commun.* **137**, 936–942
 18. Schoofs, L., Holman G. M., Hayes, T. K., Nachman, R. J., Kochansky, J. P., and De Loof, A. (1992) Isolation, identification and synthesis of locustamyotropin III and IV, two additional neuropeptides of *Locusta migratoria*: members of the locustamyotropin peptide family. *Insect Biochem. Mol. Biol.* **22**, 447–452
 19. Žďárek, J., Nachman, R. J., and Hayes, T. K. (1998) Structure-activity relationships of insect neuropeptides of the pyrokinin/PBAN family and their selective action on pupariation in fleshfly (*Neobellera bullata*) larvae (Diptera:Sarcophagidae). *Eur. J. Entomol.* **95**, 9–16
 20. Choi, M. Y., Fuerst, E. J., Rafaeli, A., and Jurenka R. (2003) Identification of a G protein-coupled receptor for pheromone biosynthesis activating neuropeptide from pheromone glands of the moth *Helicoverpa zea*. *Proc. Natl. Acad. Sci. U. S. A.* **100**, 9721–9726
 21. Howard, A. D., Wang, R., Pong, S. S., Mellin, T. N., Strack, A., Guan, X. M., Zeng, Z., Williams, D.

- L. Jr., Feighner, S. D., Nunes, C. N., Murphy, B., Stair, J. N., Yu, H., Jiang, Q., Clements, M. K., Tan, C. P., McKee, K. K., Hreniuk, D. L., McDonald, T. P., Lynch, K. R., Evans, J. F., Austin, C. P., Caskey, C. T., Van der Ploeg, L. H., and Liu, Q. (2000) Identification of receptors for neuromedin U and its role in feeding. *Nature* **406**, 70–74
22. Szekeres, P. G., Muir, A. I., Spinage, L. D., Miller, J. E., Butler, S. I., Smith, A., Rennie, G. I., Murdock, P. R., Fitzgerald, L. R., Wu, H., McMillan, L. J., Guerrero, S., Vawter, L., Elshourbagy, N. A., Mooney, J. L., Bergsma, D. J., Wilson, S., and Chambers, J. K. (2000) Neuromedin U is a potent agonist at the orphan G protein-coupled receptor FM3. *J. Biol. Chem.* **275**, 20247–20250
23. Fujii, R., Hosoya, M., Fukusumi, S., Kawamata, Y., Habata, Y., Hinuma, S., Onda, H., Nishimura, O., and Fujino, M. (2000) Identification of neuromedin U as the cognate ligand of the orphan G protein-coupled receptor FM-3. *J. Biol. Chem.* **275**, 21068–21074
24. Hosoya, M., Moriya, T., Kawamata, Y., Ohkubo, S., Fujii, R., Matsui, H., Shintani, Y., Fukusumi, S., Habata, Y., Hinuma, S., Onda, H., Nishimura, O., and Fujino, M. (2000) Identification and functional characterization of a novel subtype of neuromedin U receptor. *J. Biol. Chem.* **275**, 29528–29532
25. Minamino, N., Kangawa, K., and Matsuo, H. (1985) Neuromedin U-8 and U-25: novel uterus stimulating and hypertensive peptides identified in porcine spinal cord. *Biochem. Biophys. Res. Commun.* **130**, 1078–1085
26. Mori, K., Miyazato, M., Ida, T., Murakami, N., Serino, R., Ueta, Y., Kojima, M., and Kangawa, K. (2005) Identification of neuromedin S and its possible role in the mammalian circadian oscillator system. *EMBO J.* **24**, 325–335
27. Hull, J.J., Ohnishi, A., Moto, K., Kawasaki, Y., Kurata, R., Suzuki, M. G., and Matsumoto, S. (2004) Cloning and characterization of the pheromone biosynthesis activating neuropeptide receptor from the silkworm, *Bombyx mori*: Significance of the carboxyl terminus in receptor internalization. *J. Biol. Chem.* **279**, 51500–51507
28. Kim, Y. J., Nachman, R. J., Aimanova, K., Gill, S., and Adams M. E. (2008) The pheromone biosynthesis activating neuropeptide (PBAN) receptor of *Heliothis virescens*: Identification, functional expression, and structure-activity relationships of ligand analogs. *Peptides* **29**, 268–275
29. Lee, D. W., Shrestha, S., Kim, A. Y., Park, S. J., Yang, C. Y., Kim, Y., and Koh, Y. H. (2011) RNA interference of pheromone biosynthesis-activating neuropeptide receptor suppresses mating behavior by inhibiting sex pheromone production in *Plutella xylostella* (L.). *Insect Biochem. Mol. Biol.* **41**, 236–243
30. Rafaeli, A., Bober, R., Becker, L., Choi, M.-Y., Fuerst, E.-J., and Jurenka, R. (2007) Spatial distribution and differential expression of the PBAN receptor in tissues of adult *Helicoverpa* spp. (Lepidoptera: Noctuidae). *Insect Mol. Biol.* **16**, 287–293
31. Zheng, L., Lytle, C., Njauw, C.-N., Altstein, M., and Martins-Green, M. (2007) Cloning and characterization of the pheromone biosynthesis activating neuropeptide receptor gene in *Spodoptera*

littoralis larvae. *Gene* **393**, 20–30

32. Cheng, Y., Luo, L., Jiang, X., Zhang, L., and Niu, C. (2010) Expression of pheromone biosynthesis activating neuropeptide and its receptor (PBANR) mRNA in adult female *Spodoptera exigua* (Lepidoptera: Noctuidae). *Arch Insect Biochem. Physiol.* **75**, 13–27
33. Lee, J. M., Hull, J. J., Kawai, T., Goto, C., Kurihara, M., Tanokura, M., Nagata, K., Nagasawa, H., and Matsumoto, S. (2012) Re-evaluation of the PBAN receptor molecule: characterization of PBANR variants expressed in the pheromone glands of moths. *Front. Endocrinol.* **3**, 6. doi: 10.3389/fendo.2012.00006
34. Nusawardani, T., Kroemer, J.A., Choi, M.-Y., and Jurenka, R.A. (2013) Identification and characterization of the pyrokinin/pheromone biosynthesis activating neuropeptide family of G protein-coupled receptors from *Ostrinia nubilalis*. *Insect Mol. Biol.* **22**, 331–340
35. Hull, J. J., Kajigaya, R., Imai, K., and Matsumoto, S. (2007) Sex pheromone production in the silkworm, *Bombyx mori*, is mediated by store-operated Ca²⁺ channels. *Biosci. Biotechnol. Biochem.* **71**, 1993–2001
36. Hull, J. J., Ohnishi, A., and Matsumoto, S. (2005) Regulatory mechanisms underlying pheromone biosynthesis activating neuropeptide (PBAN)-induced internalization of the *Bombyx mori* PBAN receptor. *Biochem. Biophys. Res. Commun.* **334**, 69–78
37. Hull, J. J., Lee, J. M., and Matsumoto, S. (2011) Identification of specific sites in the third intracellular loop and carboxyl terminus of the *Bombyx mori* pheromone biosynthesis activating neuropeptide receptor crucial for ligand-induced internalization. *Insect Mol. Biol.* **20**, 801–811
38. Choi, M.-Y., Fuerst, E.-J., Rafaeli, A., and Jurenka, R. A. (2007) Role of extracellular domains in PBAN/pyrokinin GPCRs from insects using chimera receptors. *Insect Biochem. Mol. Biol.* **37**, 296–306
39. Choi, M.-Y., and Jurenka, R. A. (2010) Site-directed mutagenesis and PBAN activation of the *Helicoverpa zea* PBAN-receptor. *FEBS Lett.* **584**, 1212–1216
40. Stern, P. S., Yu, L., Choi, M.-Y., Jurenka, R. A., Becker, L., and Rafaeli, A. (2007) Molecular modeling of the binding of pheromone biosynthesis activating neuropeptide to its receptor. *J. Insect Physiol.* **53**, 803–818
41. Jurenka, R., and Nusawardani, T. (2011) The pyrokinin/pheromone biosynthesis-activating neuropeptide (PBAN) family of peptides and their receptors in Insecta: evolutionary trace indicates potential receptor ligand-binding domains. *Insect Mol. Biol.* **20**, 323–334
42. Nachman, R. J., Kuniyoshi, H., Roberts, V. A., Holman, G. M., and Suzuki, A. (1993) Active conformation of the pyrokinin/PBAN neuropeptide family for pheromone biosynthesis in the silkworm. *Biochem. Biophys. Res. Commun.* **193**, 661–666
43. Clark, B. A., and Prestwich, G. D. (1996) Evidence for a C-terminal turn in PBAN. An NMR and distance geometry study. *Int. J. Pept. Protein Res.* **47**, 361–368

44. Nagata, K., Okada, A., Kawai, T., Ohtsuka, J., Hull, J. J., Moto, K., Matsumoto, S., Nagasawa, H., and Tanokura, M. (2009) NMR solution structure analysis of the C-terminal linear and cyclic peptides of pheromone biosynthesis-activating neuropeptide (PBAN) from the silkworm *Bombyx mori* in *Peptides: Breaking Away: Proceedings of the 21st American Peptide Symposium* (Lebl, M. ed.), American Peptide Society, Prompt Scientific Publishing, San Diego. pp 345–346
45. Nielsen, M., Lundegaard, C., Lund, O., and Petersen, T. N. (2010) CPHmodels-3.0—remote homology modeling using structure-guided sequence profiles. *Nucl. Acids Res.* **38**, W576–W 581
46. Lambert, C., Leonard, N., De Bolle, X., and Depiereux, E. (2002) ESyPred3D: prediction of proteins 3D structures. *Bioinformatics* **18**, 1250–1256
47. Kelley, L. A., and Sternberg, M. J. E. (2009) Protein structure prediction on the web: a case study using the Phyre server. *Nat. Protocols* **4**, 363–371
48. Cherezov, V., Rosenbaum, D. M., Hanson, M. A., Rasmussen, S. G., Thian, F. S., Kobilka, T. S., Choi, H. J., Kuhn, P., Weis, W. I., Kobilka, B. K., and Stevens, R. C. (2007) High-resolution crystal structure of an engineered human β_2 -adrenergic G protein-coupled receptor. *Science* **318**, 1258–1265
49. Hanson, M. A., Cherezov, V., Griffith, M. T., Roth, C. B., Jaakola, V. P., Chien, E. Y., Velasquez, J., Kuhn, P., and Stevens, R. C. (2008) A specific cholesterol binding site is established by the 2.8 Å structure of the human β_2 -adrenergic receptor. *Structure* **16**, 897–905
50. Jaakola, V. P., Griffith, M. T., Hanson, M. A., Cherezov, V., Chien, E. Y., Lane, J. R., Ijzerman, A. P., and Stevens, R. C. (2008) The 2.6 angstrom crystal structure of a human A_{2A} adenosine receptor bound to an antagonist. *Science* **322**, 1211–1217
51. Larkin, M. A., Blackshields, G., Brown, N. P., Chenna, R., McGettigan, P. A., McWilliam, H., Valentin, F., Wallace, I. M., Wilm, A., Lopez, R., Thompson, J. D., Gibson, T. J., and Higgins, D. G. (2007). ClustalW and ClustalX version 2.0. *Bioinformatics* **23**, 2947–2948
52. Homma, T., Watanabe, K., Tsurumaru, S., Kataoka, H., Imai, K., Kamba, M., Niimi, T., Yamashita, O., and Yaginuma, T. (2006) G protein-coupled receptor for diapause hormone, an inducer of *Bombyx* embryonic diapause. *Biochem. Biophys. Res. Commun.* **344**, 386–393
53. Cazzamali, G., Torp, M., Hauser, F., Williamson, M., and Grimmekhuijzen, C. J. (2005) The *Drosophila* gene CG9918 codes for a pyrokinin-1 receptor. *Biochem. Biophys. Res. Commun.* **335**, 14–19
54. Rosenkilde, C., Cazzamali, G., Williamson, M., Hauser, F., Søndergaard, L., DeLotto, R., and Grimmekhuijzen, C. J. (2003) Molecular cloning, functional expression, and gene silencing of two *Drosophila* receptors for the *Drosophila* neuropeptide pyrokinin-2. *Biochem. Biophys. Res. Commun.* **309**, 485–494
55. Hasegawa, H., and Holm, L. (2009) Advances and pitfalls of protein structural alignment. *Curr. Opin. Struct. Biol.* **19**, 341–348.

56. Cook, L. L., and Gafni, A. (1988) Protection of phosphoglycerate kinase against in vitro aging by selective cysteine methylation. *J. Biol. Chem.* **263**, 13991–13993
57. Vaughn, J. L., Goodwin, R. H., Tompkins, G. J., and McCawley, P. (1977) The establishment of two cell lines from the insect *Spodoptera frugiperda* (Lepidoptera; Noctuidae). *In Vitro* **13**, 213–217
58. Smith, G. E., Ju, G., Ericson, B. L., Moschera, J., Lahm, H. W., Chizzonite, R., and Summers, M. D. (1985) Modification and secretion of human interleukin 2 produced in insect cells by a baculovirus expression vector. *Proc. Natl. Acad. Sci. U. S. A.* **82**, 8404–8408
59. Bylund, D. B., Deupree, J. D., and Toews, M. L. (2004) Radioligand-binding methods for membrane preparations and intact cells. *Methods Mol. Biol.* **259**, 1–28
60. Warne, A., Moukhametzianov, R., Baker, J. G., Nehmé, R., Edwards, P. C., Leslie, A. G., Schertler, G. F., and Tate, C. G. (2011) The structural basis for agonist and partial agonist action on a β_1 -adrenergic receptor. *Nature* **469**, 241–244
61. Xu, F., Wu, H., Katritch, V., Han, G. W., Jacobson, K. A., Gao, Z. G., Cherezov, V., and Stevens, R. C. (2011) Structure of an agonist-bound human A_{2A} adenosine receptor. *Science* **332**, 322–327
62. Trott, O., and Olson, A. J. (2010) AutoDock Vina: improving the speed and accuracy of docking with a new scoring function, efficient optimization, and multithreading. *J. Comp. Chem.* **31**, 455–461
63. Krissinel, E., and Henrick, K. (2007) Inference of macromolecular assemblies from crystalline state. *J. Mol. Biol.* **372**, 774–797
64. DeLano, W. L. (2002) PyMOL: an open-source molecular graphics tool. *CCP4 Newslett. Protein Crystallogr.* **40**, 44–53.
65. Chien, E. Y., Liu, W., Zhao, Q., Katritch, V., Han, G. W., Hanson, M. A., Shi, L., Newman, A. H., Javitch, J. A., Cherezov, V., and Stevens, R. C. (2010) Structure of the human dopamine D3 receptor in complex with a D2/D3 selective antagonist. *Science* **330**, 1091–1095
66. White, J. F., Noinaj, N., Shibata, Y., Love, J., Kloss, B., Xu, F., Gvozdenovic-Jeremic, J., Shah, P., Shiloach, J., Tate, C. G., and Grisshammer, R. (2012) Structure of the agonist-bound neurotensin receptor. *Nature* **490**, 508–513
67. Kobilka, B. K., Kobilka, T. S., Daniel, K., Regan, J. W., Caron, M. G., and Lefkowitz, R. J. (1988) Chimeric α_2 - β_2 -adrenergic receptors: delineation of domains involved in effector coupling and ligand binding specificity. *Science* **240**, 1310–1316
68. Brighton, P. J., Szekeres, P. G., and Willars, G. B. (2004) Neuromedin U and its receptors: structure, function, and physiological roles. *Pharmacol. Rev.* **56**, 231–248
69. Kawai, T., Nagata, K., Okada, K., Hayakawa, K., Hull, J. J., Lee, H. M., Matsumoto, S., Tanokura, M., and Nagasawa, H. (2011) Structure-activity relationship studies of the pheromone biosynthesis-activating neuropeptide of silkworm, *Bombyx mori* in *Peptide science 2010: Proceedings of the Fifth International Peptide Symposium* (Fujii, N. and Kiso, Y. eds.), The Japanese Peptide Society, Osaka. p 126

70. Kawai, T., Lee, J. M., Nagata, K., Matsumoto, S. Tanokura, M., and Nagasawa, H. (2012) The arginine residue within the C-terminal active core of *Bombyx mori* pheromone biosynthesis-activating neuropeptide (PBAN) is essential for receptor binding and activation. *Front. Endocrinol.* **3**, 42. doi: 10.3389/fendo.2012.00042
71. Hewes, R. S., and Taghert, P. H. (2001) Neuropeptides and neuropeptide receptors in the *Drosophila melanogaster* genome. *Genome Res.* **11**, 1126–1142
72. Park, Y., Kim, Y.-J., and Adams, M. E. (2002) Identification of G protein-coupled receptors for *Drosophila* PRXamide peptides, CCAP, corazonin, and AKH supports a theory of ligand-receptor coevolution. *Proc. Natl. Acad. Sci. U. S. A.* **99**, 11423–11428
73. Congreve, M., Langmead, C. J., Mason, J. S., and Marshall, F. H. (2011) Progress in structure based drug design for G protein-coupled receptors. *J. Med. Chem.* **54**, 4283–4311.
74. Sabio, M., Jones, K., and Topiol, S. (2008) Use of the X-ray structure of the β_2 -adrenergic receptor for drug discovery. Part 2: Identification of active compounds. *Bioorg. Med. Chem. Lett.* **18**, 5391–5395
75. Mobarec, J. C., Sanchez, R., and Filizola, M. (2009) Modern homology modeling of G-protein coupled receptors: which structural template to use? *J. Med. Chem.* **52**, 5207–5216
76. Thomas, C. J., Brown, H. L., Hawes, C. R., Lee, B. Y., Min, M. K., King, L. A., and Possee, R. D. (1998) Localization of a baculovirus-induced chitinase in the insect cell endoplasmic reticulum. *J. Virol.* **72**, 10207–10212
77. Holst, B., Nygaard, R., Valentin-Hansen, L., Bach, A., Engelstoft, M. S., Petersen, P. S., Frimurer, T. M., and Schwartz, T. W. (2010) A conserved aromatic lock for the tryptophan rotameric switch in TM-VI of seven-transmembrane receptors. *J. Biol. Chem.* **285**, 3973–3985
78. Kawano, T., Kataoka, H., Nagasawa, H., Isogai, A., and Suzuki, A. (1992) cDNA cloning and sequence determination of the pheromone biosynthesis activating neuropeptide of the silkworm, *Bombyx mori*. *Biochem. Biophys. Res. Commun.* **189**, 221–226
79. Jones, D. T. (2007) Improving the accuracy of transmembrane protein topology prediction using evolutionary information. *Bioinformatics* **23**, 538–544

Acknowledgments—We thank Akinori Suzuki (formerly Akita Prefectural University), Teruhiko Beppu (Nihon University), Harushi Nakajima (Meiji University), Naoto Minamino (National Cerebral and Cardiovascular Center), Yasuyuki Higashijima (Kyushu University), Tsuyoshi Kawano (Tottori University), Hisato Kuniyoshi (Hiroshima University), and Hidekazu Katayama (Tokai University) for discussion, encouragement and advice.

FOOTNOTES

* This work was partly supported by the Targeted Proteins Research Project (TPRP) and the Platform for Drug Discovery, Informatics and Structural Life Science of the Ministry of Education, Culture, Sports, Science, and Technology (MEXT) of Japan, and a Grant-in-Aid for Young Scientists (A) (17681026) from the Japan Society for the Promotion of Science (JSPS). Mention of trade names or commercial products in this article is solely for the purpose of providing specific information and does not imply recommendation or endorsement by the U. S. Department of Agriculture. USDA is an equal opportunity provider and employer.

¹ These authors contributed equally to this work.

² To whom correspondence should be addressed:

Masaru Tanokura, Department of Applied Biological Chemistry, Graduate School of Agricultural and Life Sciences, The University of Tokyo, 1-1-1 Yayoi, Bunkyo-ku, Tokyo 113-8657, Japan. Tel: +81-3-5841-5165; Fax: +81-3-5841-8023; E-mail: amtanok@mail.ecc.u-tokyo.ac.jp.

Koji Nagata, Department of Applied Biological Chemistry, Graduate School of Agricultural and Life Sciences, The University of Tokyo, 1-1-1 Yayoi, Bunkyo-ku, Tokyo 113-8657, Japan. Tel: +81-3-5841-2283; Fax: +81-3-5841-2283; E-mail: aknagata@mail.ecc.u-tokyo.ac.jp.

³ The abbreviations used are: A_{2A}AR, A_{2A} adenosine receptor; β 1AR, β 1 adrenergic receptor; β 2AR, β 2 adrenergic receptor; B_{\max} , density of binding sites; C5NMU, C-terminal 5-residue fragment of neuromedin U; C5PBAN, C-terminal 5-residue fragment of pheromone biosynthesis-activating neuropeptide; C10PBAN, C-terminal 10-residue fragment of PBAN; C10PBAN^{R2K}, C-terminal 10-residue fragment of PBAN with an R2K mutation; DH, diapause hormone; DHR, DH receptor; DMF, *N,N*-dimethylformamide; EC₅₀, effective concentration, 50%; ECL, extracellular loop; EGFP, enhanced green fluorescent protein; FBS, fetal bovine serum; GPCR, G-protein-coupled receptor; K_d , equilibrium dissociation constant; NMS, neuromedin S; NMU, neuromedin U; NMUR, neuromedin U receptor; NMUR1, neuromedin U receptor 1; NMUR2, neuromedin U receptor 2; NTS, neurotensin; NTSR1, neurotensin receptor 1; PBAN, pheromone biosynthesis-activating neuropeptide; PBANR, PBAN receptor; PDB, Protein Data Bank; PK, pyrokinin; PK1R, pyrokinin 1 receptor; PK2R, pyrokinin 2 receptor; RR, Rhodamine Red-X; SD, standard deviation; TCEP, tris(2-carboxyethyl)phosphine; TFA, trifluoroacetic acid; TM, transmembrane helix.

FIGURE LEGENDS

Fig. 1. Schematic diagram of *B. mori* PBANR. Ala substituted amino acid residues are shaded in black. Transmembrane domains were predicted by MEMSAT (79).

Fig. 2. Confocal imaging of Sf9 cells expressing PBANR-EGFP and Ala substitutions after incubation with 100 nM RR-C10PBAN^{R2K}. Co-localization of PBANR-EGFP and RR-C10PBAN^{R2K} is indicated by yellow in the merged images.

Fig. 3. Fluorescence-based analyses of receptor expression levels and ligand binding in cells expressing PBANR-EGFP and various Ala substitution mutants. (A) EGFP-associated fluorescence intensity of PBANR-EGFP and Ala substitutions per cell. (B) Fluorescence intensity ratio (RR/EGFP) at a ligand (C10PBAN^{R2K}) concentration of 100 nM. In (A) and (B), bars represent the mean + SD of four replicates. Different letters indicate significant difference at $P < 0.01$ by the Tukey–Kramer test. (C) Tritium-labeled C10PBAN^{R2K} ligand binding isotherms of wildtype PBANR-EGFP (WT) and three Ala substitutions (E95A, I113A and E120A).

Fig. 4. Effects of Ala substitutions on Ca^{2+} mobilization in cultured Sf9 cells. Cells transiently expressing PBANR-EGFP mutants were loaded with Fura Red-AM and then challenged with C10PBAN^{R2K}. (A) An example of the C10PBAN^{R2K}-mediated Fura-Red AM fluorescence response curve in cells transiently expressing PBANR-EGFP. (B) Concentration-response relationship of C10PBAN^{R2K} on Sf9 cells transiently expressing wildtype PBANR-EGFP or native Sf9 cells. (C) Relative Ca^{2+} response of cells transiently expressing PBAN-EGFP mutants compared to PBANR-EGFP expressing cells following incubation with varying concentrations (1, 10, and 100 nM) of C10PBAN^{R2K}. Error bars represent the mean + SD of five replicates. Different letters (a–e) indicate significant difference at $P < 0.01$ by the Tukey–Kramer test.

Fig. 5. Location of functionally important residues in PBANR. The important residues identified by Ala substitution for (A) plasma membrane localization, (B) C10PBAN^{R2K} binding, and (C) Ca^{2+} mobilization are colored and labeled in the homology-based model of PBANR. Residues shown in darker colors are more important than those depicted in lighter colors. (D) Functionally important residues in PBANR and their corresponding residues in PBANR-like class-A GPCRs and class-A GPCRs whose agonist-bound crystal structures have been solved. Biological functions affected by Ala substitution of the PBANR residues are indicated by the colored circles (localization – green; ligand binding – blue; signaling – red). Amino acid residues completely conserved with PBANR are highlighted using the same color scheme but with purple to indicate residues involved in both ligand binding and signaling. Residues shown to form

contact points with bound ligand in the solved crystal structures are indicated by solid boxes while those predicted in the docking simulations are indicated by dotted lines.

Fig 6. Docking models of C5PBAN-PBANR and C5NMU-NMUR1. (A) C5PBAN (green) docked to PBANR and (B) C5NMU (cyan) docked to NMUR1. The functionally important residues of PBANR and NMUR1 are colored orange and red, respectively, and labeled in black. This figure was prepared with PyMOL (64). (C) The contact map between the ligand residues and the receptor residues in the docking models of C5PBAN-PBANR and C5NMU-NMUR1. If a ligand residue and a receptor residue are in contact with each other, the corresponding box is highlighted green (C5PBAN-PBANR) or blue (C5NMU-NMUR1). This figure was prepared based on the output from an intermolecular interaction analysis using PISA (63).

Fig. 7. Comparison of agonist-GPCR interactions. Docking models of (A) C5PBAN-PBANR and (B) C5NMU-NMUR1. Crystal structures of (C) isoprenaline-bound β 1AR (PDB: 2Y03), (D) UK-432097-bound A_{2A}AR (PDB: 3QAK) and (E) NTS (8–13)-bound NTSR1 (PDB: 4GRV). The bound ligands are depicted as space-filling models. The docking models of C5PBAN and C5NMU are colored green and cyan, respectively, while the bound ligands in the crystal structures are colored red.

Fig. 1

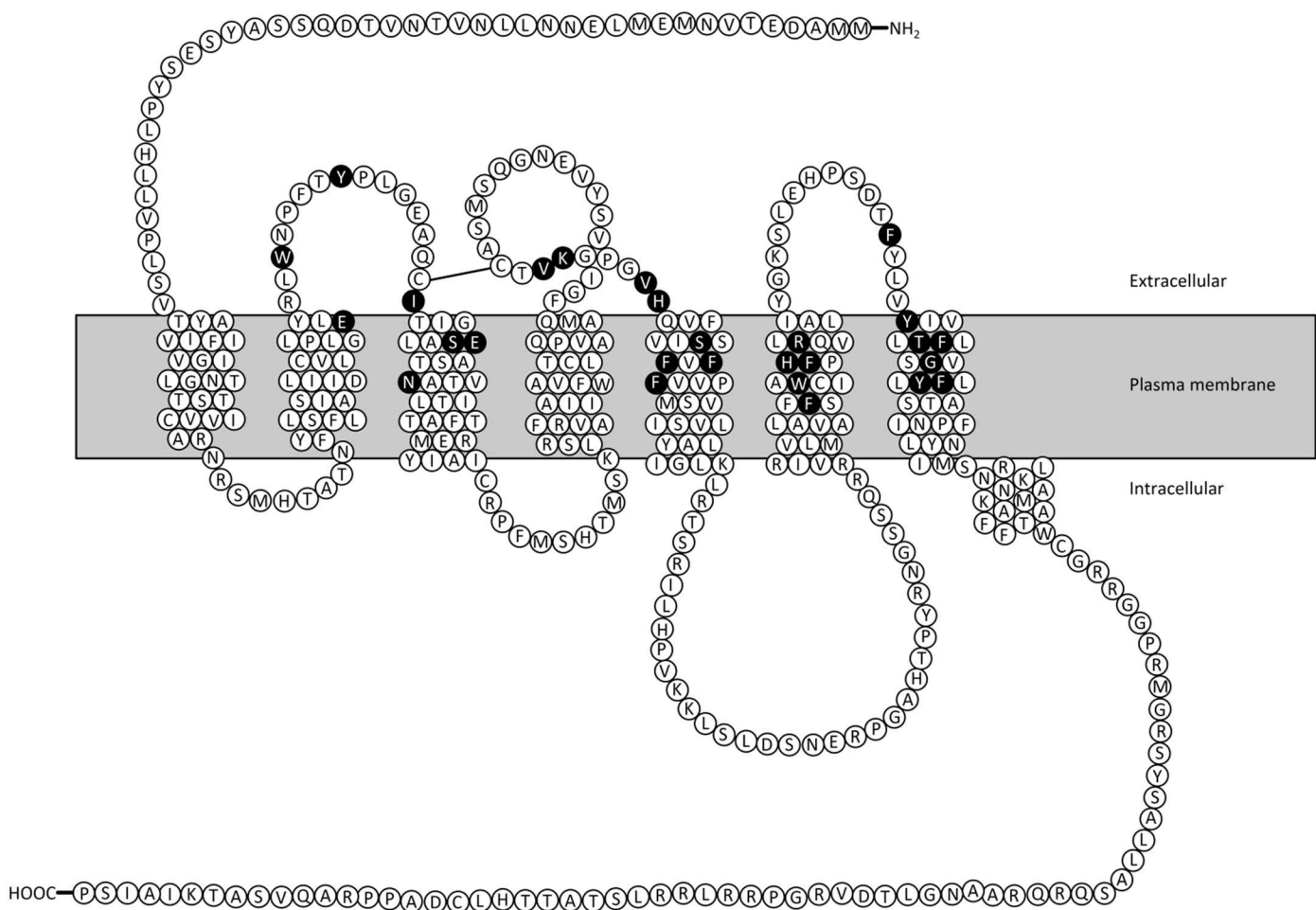


Fig. 2

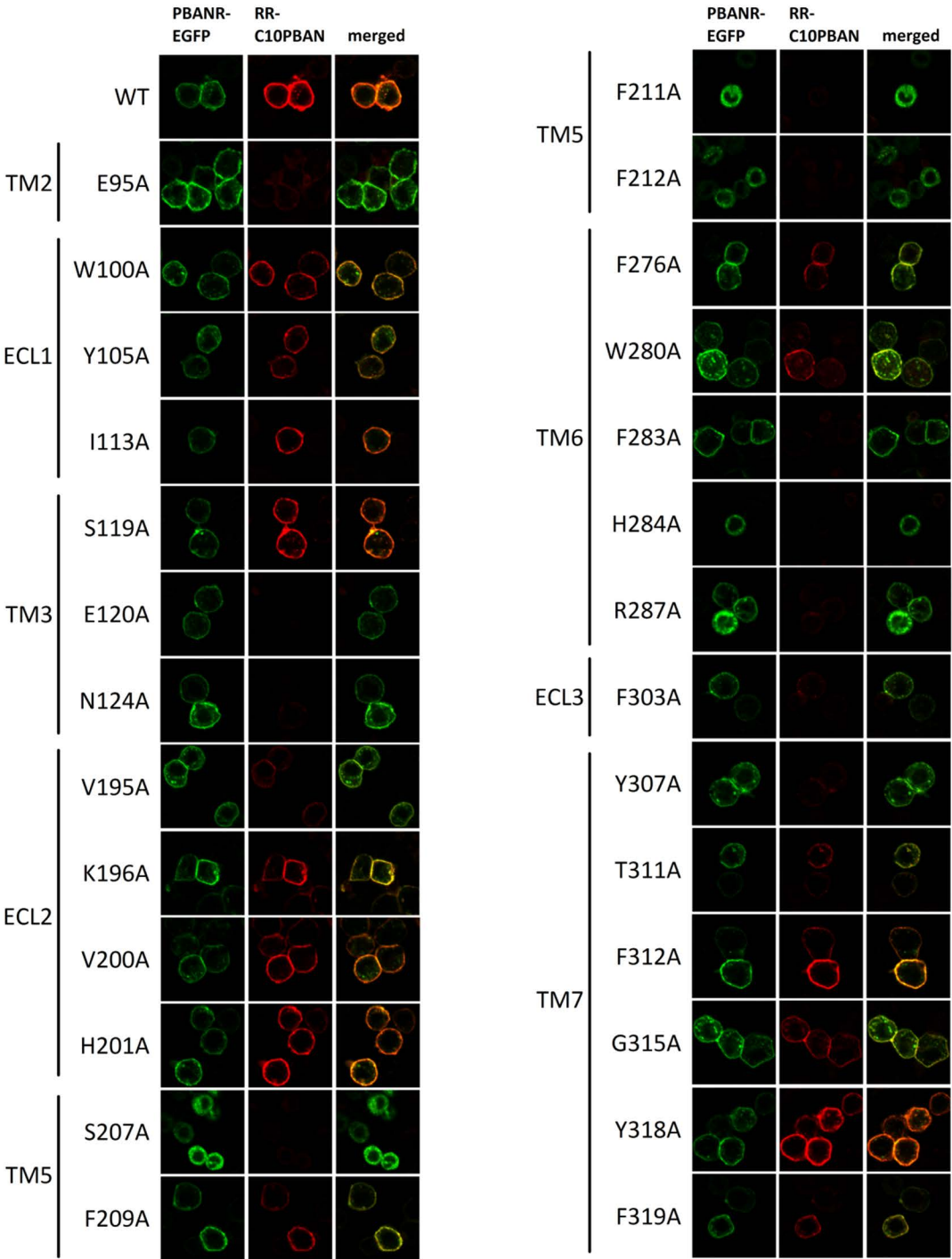


Fig. 3

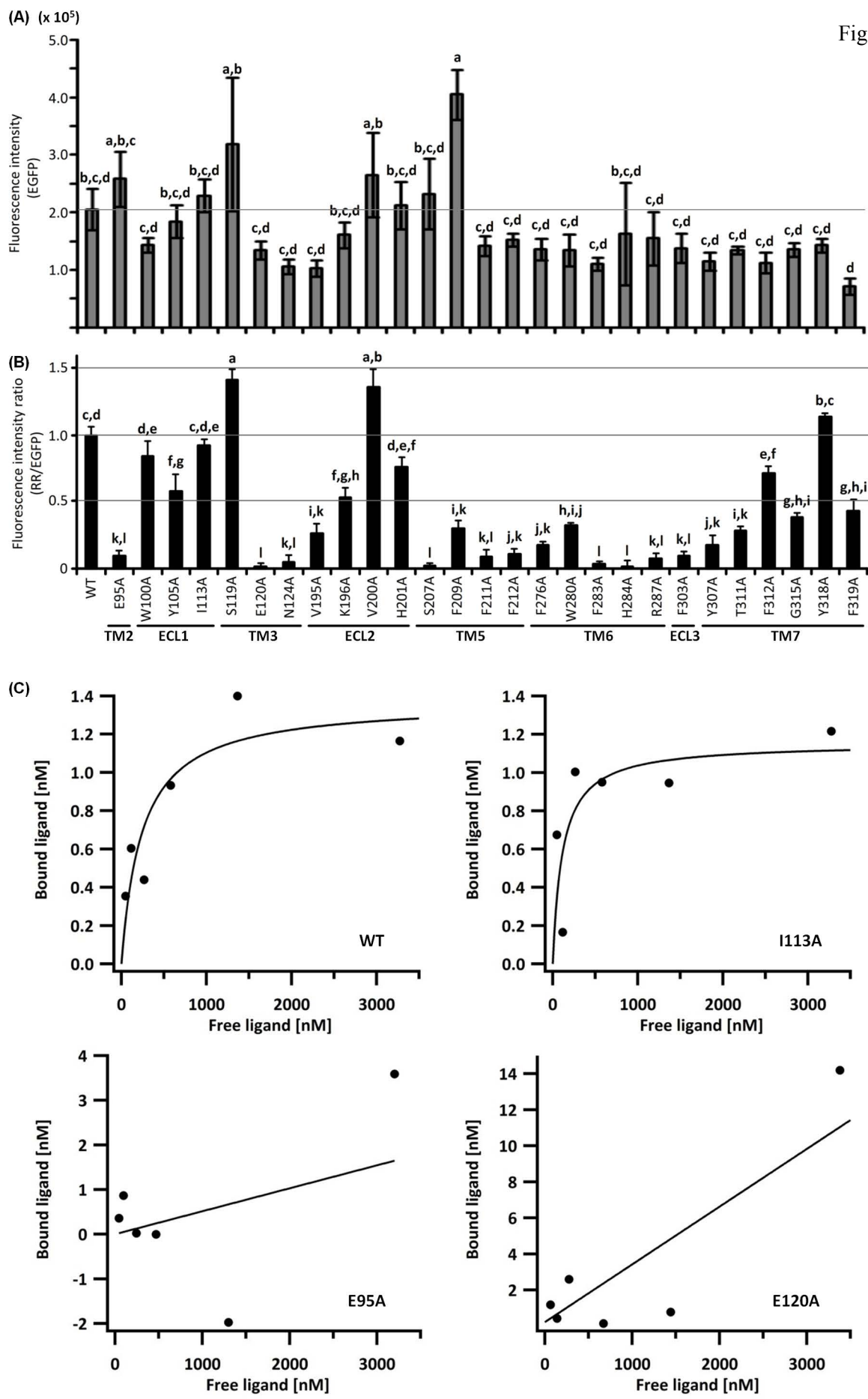


Fig. 4

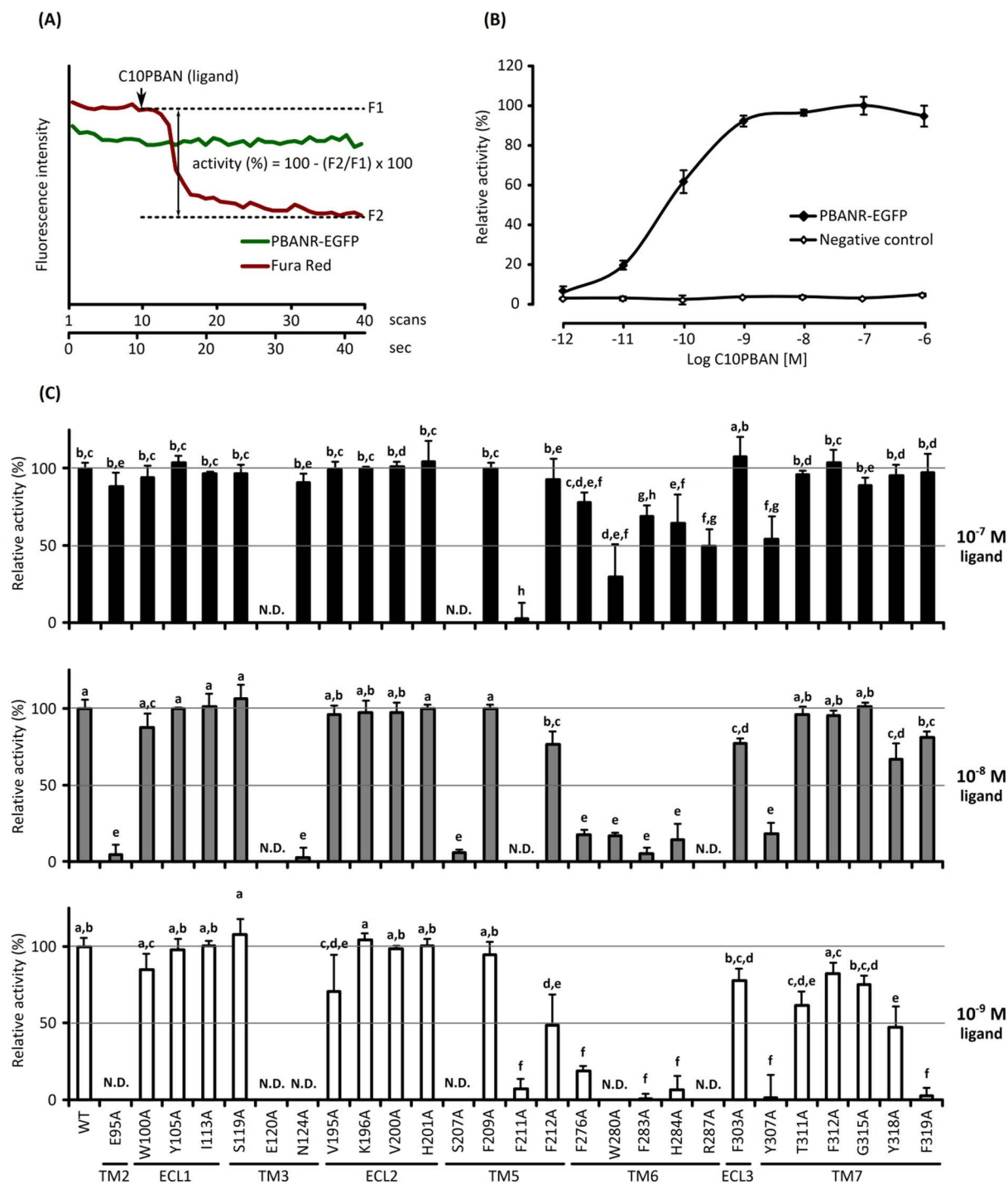
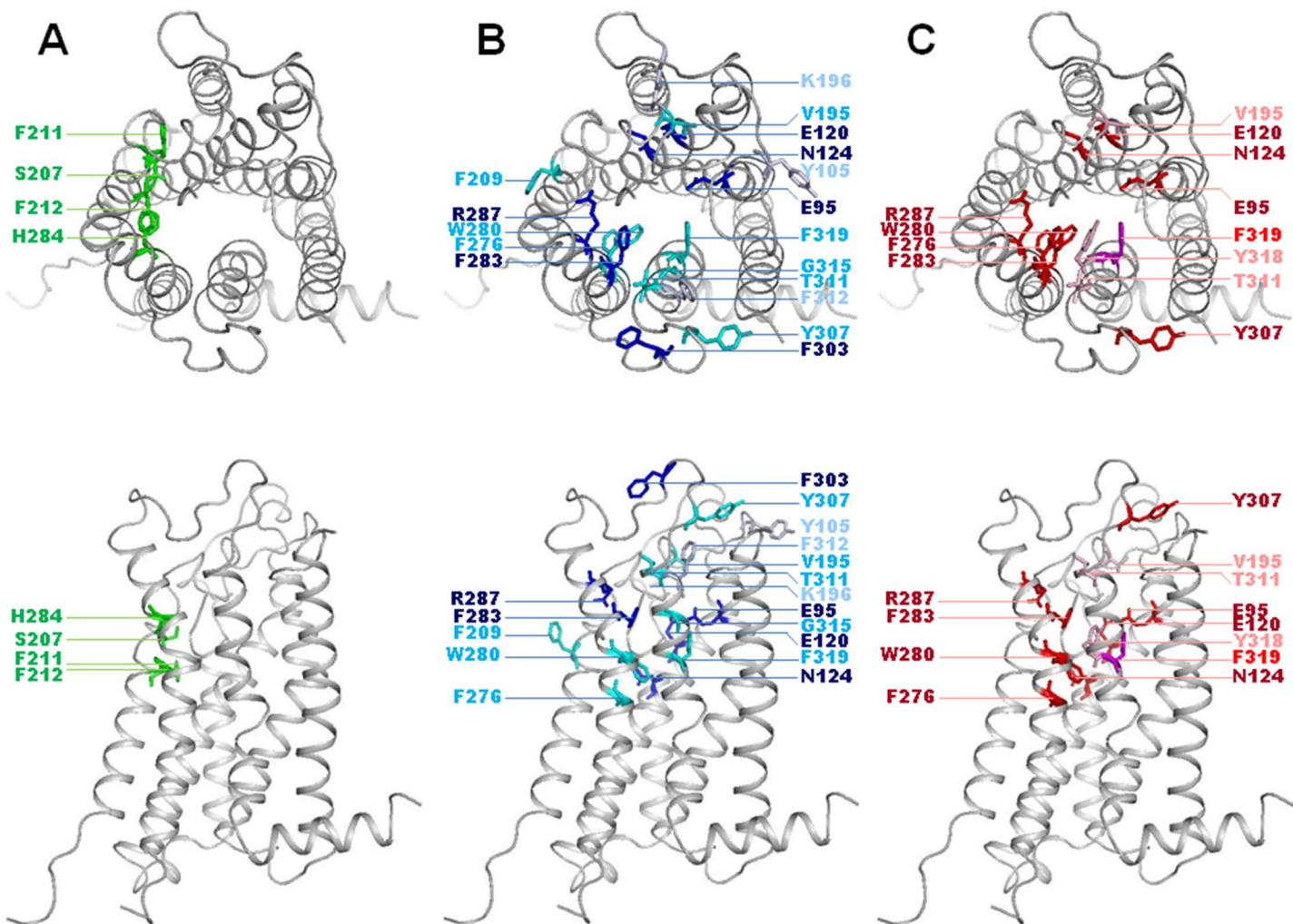


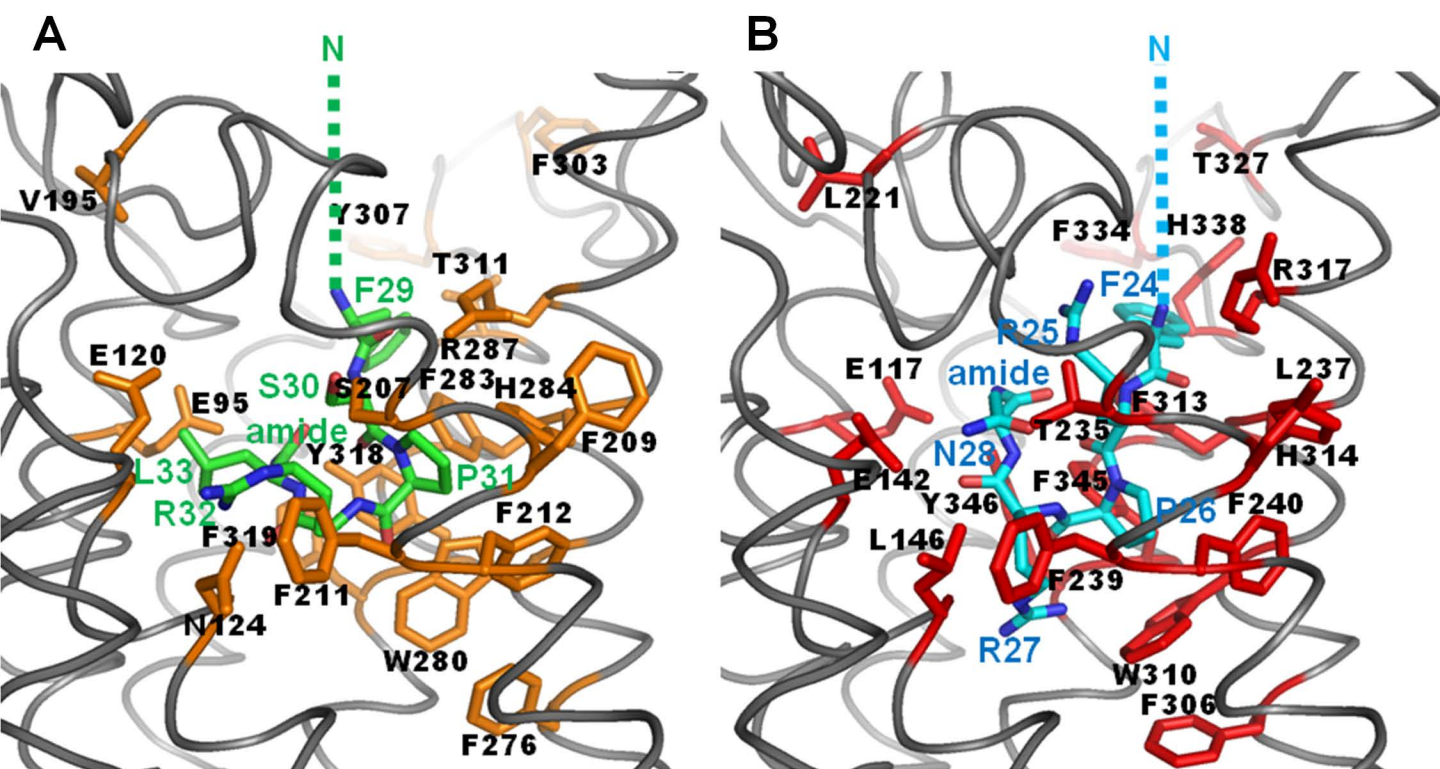
Fig. 5



D

Region	TM2	TM3	TM3	ECL2	TM5	TM5	TM5	TM5	TM6	TM6	TM6	TM6	TM6	ECL3	TM7	TM7	TM7	TM7	TM7
Residue	E95	E120	N124	V195	S207	F209	F211	F212	F276	W280	F283	H284	R287	F303	Y307	T311	G315	Y318	F319
Localization					●		●	●				●							
Ligand binding	●	●	●	●	-	●	-	-	●	●	●	-	●	●	●	●	●		●
Signaling	●	●	●	●	-		-	-	●	●	●	-	●		●	●			●
BomPBANR	E	E	N	V	S	F	F	F	F	W	F	H	R	F	Y	T	G	Y	F
HezPBANR	E	E	N	V	S	F	F	F	F	W	F	H	R	F	Y	T	G	Y	F
BomDHR	E	E	N	Q	S	F	F	F	F	W	F	H	R	P	Y	T	G	Y	Y
DmPK1R	E	E	N	I	S	F	F	F	F	W	F	H	R	Q	Y	T	G	Y	Y
DmPK2R	E	E	N	M	S	F	F	F	F	W	F	H	R	R	F	D	G	Y	F
HosNMUR1	E	E	L	L	T	L	F	F	F	W	F	H	R	T	F	H	G	F	Y
HosNMUR2	E	E	F	V	T	F	F	Y	F	W	F	H	R	S	F	H	G	F	Y
RanNTSR1	E	D	Y	P	N	F	S	F	F	W	Y	H	R	T	F	F	T	L	F
HosA _{2A} AR	A	L	Q	F	N	F	C	V	F	W	L	H	N	-	-	M	I	S	H
Megβ1AR	G	V	T	F	S	I	S	F	F	W	F	F	N	-	-	F	N	G	Y
Hosβ2AR	G	V	T	F	S	I	S	F	F	W	F	F	N	-	-	Y	N	G	Y
HosD3DR	V	V	T	I	S	V	S	F	F	W	F	F	H	-	-	Y	T	G	Y

Fig. 6



C

[illegible]

Fig. 7

